Rayleigh scattering in a liquid far from thermal equilibrium

P. N. Segrè, R. W. Gammon, and J. V. Sengers
Institute for Physical Science and Technology, University of Maryland, College Park, Maryland 20742

B. M. Law
Department of Physics, Kansas State University, Manhattan, Kansas 66506
(Received 19 August 1991)

We report the results of Rayleigh-scattering experiments in liquid toulene that is subjected to a stationary temperature gradient, but which otherwise is kept in a quiescent state. The measurements were made with temperature gradients up to 224 K/cm and scattering angles down to 0.45°. They probe fluctuations with wavelengths up to 40 μm and demonstrate the presence of long-range fluctuations in a nonequilibrium liquid. The strength of the observed nonequilibrium heat-mode and viscous-mode fluctuations varies with the square of the temperature gradient and with the fourth power of the wavelength of the fluctuations, in agreement with the behavior predicted by fluctuating hydrodynamics.

PACS number(s): 05.40.+j, 44.90.+c, 47.90.+a, 66.20.+d

I. INTRODUCTION

The theory of fluctuations in fluids that are in macroscopic thermodynamic equilibrium is well established. The strength and the time dependence of density fluctuations can be investigated experimentally by measuring the intensity and spectrum of scattered light. The light-scattering spectrum consists of the well-known Rayleigh-Brillouin triplet. Two symmetric Brillouin lines with shifted frequencies arise from scattering by propagating sound modes and the unshifted Rayleigh line arises from scattering by nonpropagating entropy fluctuations [1]. An interesting question is how these fluctuations are modified when the fluid is subjected to a steady temperature gradient. The relevant theoretical predictions have been reviewed by Fox [2], Tremblay [3], and more recently by Schmitz [4]. In first approximation a temperature gradient causes an asymmetry in the Brillouin lines, since the two corresponding sound modes probe regions with different temperatures. This effect is proportional to the temperature gradient ∇T and becomes largest for the sound waves propagating parallel and antiparallel to the direction of the temperature gradient. An asymmetry of the Brillouin lines induced by a thermal gradient has been observed experimentally [5,6], but the interpretation of such Brillouin-scattering measurements is complicated by the presence of boundary effects that cannot be readily eliminated in practice [4,7–10]. In the same approximation the Rayleigh line is unaffected, since the nonpropagating thermal fluctuations do not depend on the direction of the temperature gradient. For the Rayleigh spectrum to be modified, the imposed temperature gradient has to be large enough so that quadratic effects become observable. Hence we refer to this situation as the state far from thermal equilibrium [10,11].

The currently accepted theoretical expression for the effect of a temperature gradient on the Rayleigh spectrum was first derived by Kirkpatrick, Cohen, and Dorfman [11]. They demonstrated that the Rayleigh line was modified as the result of mode-coupling effects similar to those originally shown to be responsible for the nonclassical slowing down of the order-parameter fluctuations in a system near the critical point [12,13] and subsequently shown to induce asymptotic long-time-tail behavior of the molecular correlation functions in fluids in thermodynamic equilibrium [14]. As originally noticed by Ronis and Procaccia [15] and confirmed by others [4,16–18] the same expression for the Rayleigh spectrum in the presence of a temperature gradient can be obtained by a direct application of the fluctuating-hydrodynamics equations to a nonequilibrium fluid.

It turns out that the presence of a temperature gradient gives rise to a coupling between the entropy fluctuations and the transverse-momentum fluctuations, i.e., a coupling between the heat mode and the viscous mode. As a consequence, the Rayleigh line contains an enhanced nonequilibrium heat-mode contribution whose relaxation is governed by the thermal diffusivity as well as a nonequilibrium viscous-mode contribution whose relaxation is governed by the kinematic viscosity. Both contributions are proportional to the square of the temperature gradient ∇T and inversely proportional to the fourth power of the wave number q of the fluctuations.

This rapid growth of the strength of the fluctuations with the wavelengths is a striking phenomenon not present in fluids in thermal equilibrium. The appearance of long-range correlations turns out to be a general phenomenon in nonequilibrium states [3,19–23], so that an experimental study of these long-range correlations has become of considerable interest.

In our laboratory we have made some attempts to measure the effects of a temperature gradient on the Rayleigh scattering [24–26]. Our first measurements confirmed the presence of both an enhanced nonequilibrium heat-mode contribution and a negative nonequilibrium viscous-mode contribution as predicted by the theory. Furthermore, both contributions are found to vary with $(\nabla T)^2/q^4$ as expected [24,25]. In subsequent experiments with an improved scattering cell we were also able to determine the amplitudes of these contributions in

good agreement with the theoretical predictions [26]. These earlier results were obtained by plotting the experimental amplitudes as a function of $(\nabla T)^2/q^4$.

Subsequently we have made further improvements in the experiment enabling us to measure the nonequilibrium Rayleigh-scattering contributions at even smaller scattering angles corresponding to wavelengths up to 40 μm. We have now obtained an extensive set of light scattering data as a function of ∇T over a substantial range of wave numbers q allowing us to evaluate the dependence of the experimental amplitudes of the nonequilibrium fluctuations on ∇T and q separately.

The paper is organized as follows. In Sec. II we review the theoretical assumptions and predictions. In Sec. III we discuss the improvements made in the experimental arrangement. In Sec. IV we present our experimental results which are compared with the theoretical predictions. We then evaluate in Sec. V possible corrections to the measurements that results from the spatial variation of the physical properties of the liquid as a result of this temperature dependence. Our conclusions are summarized in Sec. VI.

II. THEORY

Rayleigh light scattered with wave number q and frequency ω is proportional to the correlation function $\langle s_{q,\omega} s^*_{q,\omega} \rangle$, which measures the fluctuations in the specific entropy [27–29]. The effect of the presence of a temperature gradient on these entropy fluctuations can be readily derived on the basis of fluctuating hydrodynamics [4,16,17,29]. For this purpose it is convenient to use the fluctuations δs, δp, and $\delta \mathbf{v}$ in specific entropy s, pressure p, and velocity $\mathbf{v}$ as the fluctuating variables. As in the derivation of the Rayleigh-Brillouin spectrum of a system in thermodynamic equilibrium [27,28], it is sufficient to consider the linearized fluctuating hydrodynamics equations, in this case linearized around the steady state with a fixed temperature gradient ∇T. Since we consider here only the Rayleigh spectrum, we neglect the pressure fluctuations and take $\delta p = 0$. Starting from the fluctuating hydrodynamics equations, as given, for example, by Landau and Lifshitz [30], and taking the spatial and temporal Fourier transforms, one obtains [17,29]

$$(i\omega + D_T q^2)\delta s_{q,\omega} = -\left[\frac{c_p}{T}\right]\nabla T\cdot\delta\mathbf{v}_{q,\omega} - \frac{1}{\rho T} i\mathbf{q}\cdot\mathbf{g}_{q,\omega} , \quad (1)$$

$$(i\omega + \nu q^2)\delta_{q,\omega} = -\frac{1}{\rho}(\zeta + \tfrac{1}{3}\eta)\mathbf{q}(\mathbf{q}\cdot\delta\mathbf{v}_{q,\omega}) - \frac{i}{\rho}\mathbf{q}\cdot\mathbf{S}_{q,\omega} . \quad (2)$$

Here D_T is the thermal diffusivity, c_p the isobaric specific heat, ρ the density, η the shear viscosity, $\nu = \eta/\rho$ the kinematic viscosity, and ζ the bulk viscosity. In addition, $\mathbf{g}_{q,\omega}$ and $\mathbf{S}_{q,\omega}$ are the Fourier transforms of the fluctuating heat flux $\mathbf{g}$ and the fluctuating shear tensor $\mathbf{S}$ which for a system in thermodynamic equilibrium are correlated as [16,30]

$$\langle \hat{\mathbf{q}}\cdot\mathbf{g}_{q,\omega}\hat{\mathbf{q}}\cdot\mathbf{g}^*_{q',\omega'}\rangle = 2k_B T^2 \rho c_p D_T \delta(\mathbf{q}-\mathbf{q}')\delta(\omega-\omega') , \quad (3)$$

$$\langle \hat{\mathbf{q}}\cdot\mathbf{S}_{q,\omega}(1-\hat{\mathbf{q}}\hat{\mathbf{q}})\cdot\hat{\mathbf{z}}\cdot\hat{\mathbf{q}}'\cdot\mathbf{S}^*_{q',\omega'}\cdot(1-\hat{\mathbf{q}}'\hat{\mathbf{q}}')\cdot\hat{\mathbf{z}}\rangle = 2k_B T\rho\nu\delta(\mathbf{q}-\mathbf{q}')\delta(\omega-\omega') , \quad (4)$$

$$\langle g^i_{q,\omega} S^{j,k\,*}_{q,\omega}\rangle = 0 , \quad (5)$$

where k_B is Boltzmann's constant, and where the subscripts i,j,k refer to the individual components of the vector $\mathbf{g}_{k,\omega}$ and the tensor $\mathbf{S}_{k,\omega}$. In deriving Eqs. (1) and (2) we have neglected the spatial variations of the thermodynamic and transport properties induced by the temperature gradient. The effect of these spatial variations are expected to be small [15], but will be evaluated in Sec. V.

Equation (1) differs from the corresponding equations for a system in thermodynamic equilibrium by the presence of the term proportional to $\nabla T\cdot\delta\mathbf{v}$; it is this term that is responsible for the modifications of the Rayleigh spectrum due to the temperature gradient. We consider a horizontal fluid layer subject to a stationary temperature gradient $\nabla T = dT/dz$ in the $\hat{\mathbf{z}}$ direction. The scattering vector $\mathbf{q}$ is taken in a direction perpendicular to the temperature gradient ∇T, since this configuration yields the largest effect on the Rayleigh line. As demonstrated elsewhere [17], to obtain the Rayleigh spectrum we can neglect fluctuations in the longitudinal velocity and need to consider only fluctuations in the transverse velocity $\mathbf{v}^t$:

$$\delta\mathbf{v}^t_{q,\omega} = (1-\hat{\mathbf{q}}\hat{\mathbf{q}})\cdot\delta\mathbf{v}_{q,\omega} . \quad (6)$$

Solving (1) and (2) for $\delta s_{q,\omega}$ and $\delta\mathbf{v}^t_{q,\omega}$ we obtain

$$\delta s_{q,\omega} = -\frac{i\mathbf{q}\cdot\mathbf{g}_{q,\omega}}{\rho T(i\omega + D_T q^2)} - \frac{c_p \delta\mathbf{v}^t_{q,\omega}\cdot\hat{\mathbf{z}}}{T(i\omega + D_T q^2)}\frac{dT}{dz} , \quad (7)$$

$$\delta\mathbf{v}^t_{q,\omega} = -\frac{i\mathbf{q}\cdot\mathbf{S}_{q,\omega}\cdot(1-\hat{\mathbf{q}}\hat{\mathbf{q}})}{\rho(i\omega + \nu q^2)} . \quad (8)$$

An explicit expression for the entropy correlation function $\langle \delta s_{q,\omega}\delta s^*_{q,\omega}\rangle$ is obtained from (7) and (8), if we retain the expressions (3)–(5) for the correlation of the fluctuating variables:

$$\langle \delta s_{q,\omega}\delta s^*_{q,\omega}\rangle = \frac{k_B c_p}{\rho}\left[\frac{2D_T q^2}{\omega^2 + D_T^2 q^4}\right] \times \left[1 + \frac{c_p \nu}{T D_T(\omega^2 + \nu^2 q^4)}\left[\frac{dT}{dz}\right]^2\right] . \quad (9)$$

The crucial step in the derivation of (9) is the assumption that the expressions (3)–(5) for the correlations of the fluctuating quantities remain valid for a system far from thermal equilibrium. The validity of this assumption is not evident *a priori* and it has recently been questioned in the case that a diffusing Brownian particle is present in the fluid [31].

To elucidate the effect of the temperature gradient on the Rayleigh spectrum, Eq. (9) may be rewritten as

$$\langle \delta s_{q,\omega}\delta s^*_{q,\omega}\rangle = \frac{2k_B c_p}{\rho}\left[\left[1 + \frac{c_p \nu}{T D_T(\nu^2 - D_T^2)q^4}\left[\frac{dT}{dz}\right]^2\right]\frac{D_T q^2}{\omega^2 + D_T^2 q^4} - \frac{c_p}{T(\nu^2 - D_T^2)q^4}\left[\frac{dT}{dz}\right]^2 \frac{\nu q^2}{\omega^2 + \nu^2 q^4}\right] , \quad (10)$$

a result first obtained by Kirkpatrick, Cohen, and Dorfman [11]. If $\nabla T=0$, Eq. (10) reduces to the well-known expression for the fluctuations in a fluid in thermal equilibrium leading to a Rayleigh spectrum whose characteristic frequency is determined by the thermal diffusivity D_T. The effects of a temperature gradient are twofold. First, the intensity of the thermal Rayleigh line is enhanced. In addition, a second (negative) contribution in the Rayleigh spectrum appears whose characteristic frequency is determined by the kinematic viscosity ν. Both effects should be proportional to $(\nabla T)^2$ and inversely proportional to q^4.

III. EXPERIMENT

A schematic representation of the scattering experiment is shown in Fig. 1. In order to observe the effect of a temperature gradient on the intrinsic thermally excited fluctuations it is necessary to maintain the liquid in a quiescent state without any convective currents. This is accomplished by heating a 2-mm-thick horizontal fluid layer from above. In practice we were able to avoid convective flows at temperature gradients up to about 230 K/cm. The wave number q of the fluctuations probed by a light-scattering experiment is related to the scattering angle θ by the Bragg condition $q=4\pi(n/\lambda)\sin(\theta/2)$, where λ is the wavelength of the incident laser light and n is the refractive index of the liquid. Because the effect of the temperature gradient is proportional to θ^{-4}, it is necessary to perform the Rayleigh-scattering measurements at small scattering angles which need to be determined with high accuracy. Since a temperature gradient induces also a refractive-index gradient, use of horizontal incident light would lead to an appreciable uncertainty in the scattering angle because of beam bending. The problem is avoided by letting the incident light beam propagate in the direction antiparallel to the temperature gradient. A detailed description of the scattering cell has been presented in a previous publication [26]. We employ 0.5-in.-thick windows to reduce the large amount of stray light which is necessarily present at very small scattering angles. The temperature gradient is maintained by a water bath circulating cold water through the lower copper plate, and a computer-controlled resistive heater wrapped around the upper hot plate. The temperature stability on both plates is ± 0.02 K.

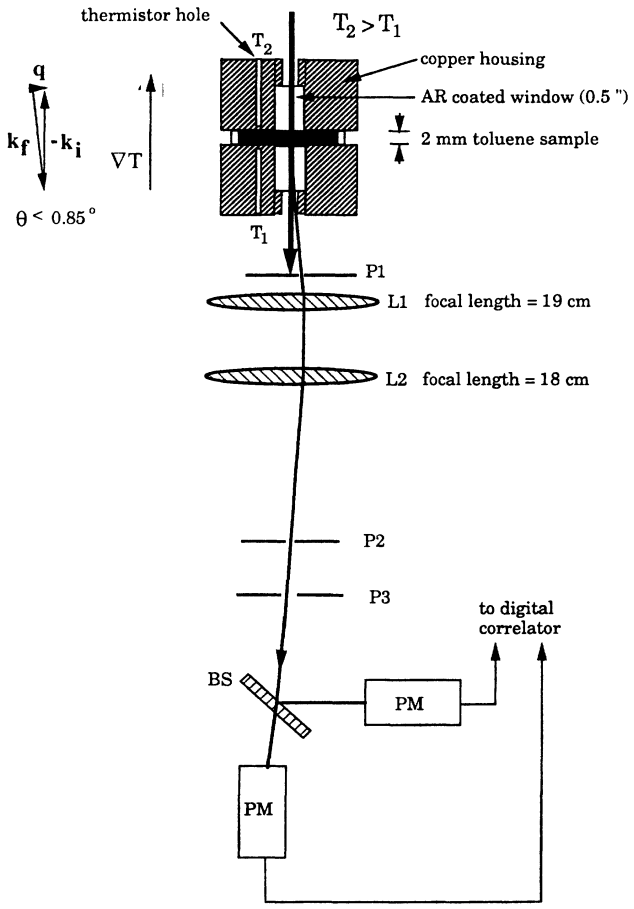

FIG. 1. Schematic representation of the experiment scattering arrangement. The temperature gradient ∇T is vertical in the direction opposite to the gravity. The incident wave vector is $\mathbf{k}_i$ and the final wave vector is $\mathbf{k}_f$. The figure also shows the location of the lenses L1 and L2; the pinholes P1, P2, and P3; a beam splitter BS; and two photomultipliers PM. AR denotes antireflective.

The time-dependent correlation function $C(q,t)$ of the scattered electric field is obtained by the heterodyne technique, where the scattered light is beat against the residual stray light [32,33]. The experimental correlation function $C(q,t)$ thus probes the entropy fluctuations as a function of the time t so that in accordance with (10),

$$C(q,t)=C_B\{1+C_0[(1+A_D)\exp(-D_Tq^2t) - A_\nu\exp(-\nu q^2t)]\}\ , \tag{11}$$

where C_0 represents the signal strength when $\nabla T=0$ and where C_B is the experimental background contribution. Furthermore, A_D and A_ν are the relative amplitudes of the nonequilibrium heat-mode and viscous-mode contributions, such that

$$A_D=A_D^*\frac{(\nabla T)^2}{q^4},\quad A_\nu=A_\nu^*\frac{(\nabla T)^2}{q^4}\ , \tag{12}$$

with

$$A_D^*=\frac{c_p}{T(\nu^2-D_T^2)}\left[\frac{\nu}{D_T}\right],\quad A_\nu^*=\frac{c_p}{T(\nu^2-D_T^2)}\ . \tag{13}$$

In practice we measure $C(q,t)$ by cross correlating the signals received by two different photomultipliers, so as to eliminate afterpulsing and thus increasing the experimental resolution at short times t [34].

In principle the wave number q can be determined from the scattering angle θ. However, an alternate and more accurate procedure is obtained by noting that for the liquid in thermal equilibrium Eq. (11) reduces to

$$C(q,t)=C_B[1+C_0e^{-D_Tq^2t}]\ . \tag{14}$$

Since we use a liquid with a known value of the thermal

diffusivity D_T, fitting the light-scattering data for $\nabla T=0$ to (14) yields q^2, in addition to C_B and C_0.

A complication arises because the measurements are not obtained at a single q value, but over a finite range of q values due to the focusing of the beam in the sample and the finite size of about 0.1° of the collection angle. This effect is usually negligible in light-scattering experiments, but becomes significant here, first because of the small scattering angles used and second because the intensity of the nonequilibrium contributions to the scattering will vary with q^4. We account for this effect by convoluting the ideal correlation function (11) with a Gaussian beam profile [35]:

$$\bar{C}(q,t)=\frac{1}{Z}\int_{q-3\delta}^{q+3\delta}dq'C(q',t)\exp\left[-\frac{(q'-q)^2}{2\delta^2}\right], \quad (15)$$

with

$$Z=\delta\sqrt{2}\pi\Phi(3\sqrt{2}), \quad (16)$$

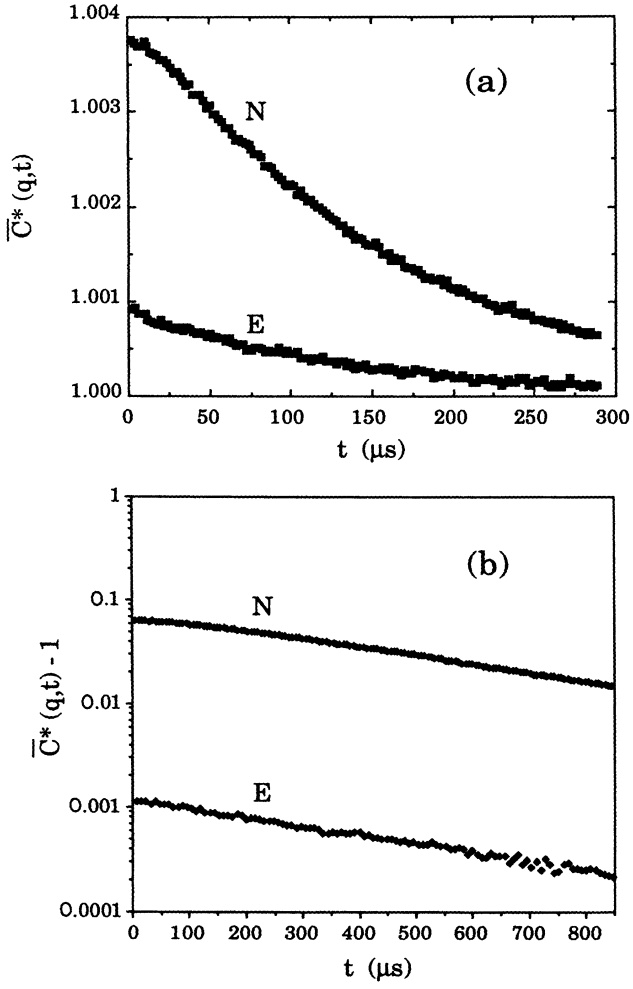

FIG. 2. Normalized experimental correlation function $\bar{C}^*(q,t)=C(q,t)/C_B$ obtained at (a) $q=2835$ cm^{-1} and (b) $q=1528$ cm^{-1}. The data labeled E were obtained with $\nabla T=0$ and the data labeled N with (a) $\nabla T=158$ K/cm and (b) $\nabla T=173$ K/cm.

where q is now the average wave number and Φ the error function, while δ is a measure of the spread of experimental wave numbers. We shall return to a discussion of this procedure in Sec. V in conjunction with the evaluation of another effect, namely that associated with spatial variations of the properties of the liquid resulting from the temperature gradient.

Typical normalized correlation functions $\bar{C}^*(q,t)=C(q,t)/C_B$, obtained at $q=2835$ and 1528 cm^{-1}, are shown in Fig. 2. The curves labeled E correspond to the equilibrium state with $\nabla T=0$ and the curves labeled N correspond to nonequilibrium states with $\nabla T=158$ and 173 K/cm. As in our previous work [24–26], the experimentally observed correlation functions clearly show a significant enhancement of the heat-mode contribution and a suppression at short times due to the negative viscous-mode contribution.

As is evident from Fig. 2(a), the observed signal strength can be as low as 0.05%, requiring long experimental collection times of several hours. Since our previous experiments we have therefore made several improvements to increase the experimental resolution. As shown in Fig. 1, pinhole P1 selects the scattering angle, while lenses L1 and L2 reimage the scattering volume onto pinhole P2. Pinholes P2 and P3 spatially filter out some of the static stray light originating from the cell windows. Our previous design for the sizes of pinholes P2 and P3 was based on ray tracing and assuming Gaussian optics. We have since included in the analysis diffraction effects which originate from the light passing through the angle selecting pinhole P1. The result is a larger focused spot size at the reimaging pinhole P2. To account for this, P2 was increased in diameter from 100 to 200 μm and P3 from 400 to 1000 μm. Another advantage of using a larger field stop P2 is a reduction in sensitivity of the experiment to possible drifts in the direction of the laser beam. In order to have an easier diffraction problem to model, the pinhole P1 was moved closer to the lens L1, and hence further from the scattering cell. This also results in a reduction of the collection aperture size δ.

An improvement was also made in the experiment by operating our Spectra-Physics 165 argon-ion laser solely in the TEM_{00} mode [36]. The degradation of spatial coherence in multiple transverse-mode operation reduces the scattered signal strength for a given input laser power. By measuring the beam intensity in the plane perpendicular to its propagation direction, we were able to profile the beam and look for the appearance of the TEM_{01}, or "doughnut" mode. By tuning the exit aperture of the laser, we could "block" out the larger radius TEM_{01} mode and gain a factor of about 2 in signal level. By projecting the laser beam on the wall, it is also possible to see with the naked eye the characteristic "snap" in the profile as the TEM_{01} mode disappears.

Further improvements in the alignment procedure were also made, and a comparison with the prior setup can be made by looking at relative signal strengths. In the previous design we typically had an incident laser power of approximately 100 mW, which produced photon count rates of approximately 100 000 s^{-1}, and fractional signal levels of 2×10^{-3} in equilibrium. We now

achieve signal levels of 4×10^{-3} at count rates of 100 000 s^{-1}, but with only 10 mW of laser power. This is an improvement by a factor of 20 in the amount of fluid scattering detected. The effect of the enlargened pinholes P2 and P3, on the other hand, is also to collect more stray light, forcing us to use a low incident laser power. While our experiments were performed with an argon-ion laser beam, at 10 mW it may become possible in the future to use a less expensive helium-neon laser. A He-Ne laser would also have the advantage of a larger wavelength and, hence, a smaller q value at a given scattering angle.

The choice of the liquid to be used in the experiment is based on the following considerations. To test the theory we need reliable values of the relevant thermodynamic and transport properties of the liquid. Furthermore, we must be able to avoid dust particles in the liquid which would yield extraneous Rayleigh-scattering contributions. For these reasons we continued to do the experiments with toluene whose thermophysical properties are known and which was kept clean as described in a previous publication [26].

IV. EXPERIMENTAL RESULTS

We have measured the scattered Rayleigh light of liquid toluene as a function of ∇T at six scattering angles ranging from 0.45° to 0.84° and corresponding to the wave numbers $q=1528$, 1663, 1811, 2034, 2122, 2255, 2484, and 2835 cm^{-1}. At each scattering angle the heterodyne correlation function of the scattered light is measured with the liquid in thermal equilibrium, i.e., $\nabla T=0$, and then with ten different values of the temperature gradient ∇T up to a maximum value of $\nabla T=224$ K/cm. In changing the temperature gradient care was taken to increase and decrease the temperatures of the upper and lower plate symmetrically, so that all experimental results correspond to the same average temperature of 40 °C. A table of the values of the relevant thermodynamic and transport properties of liquid toluene at 40 °C was presented in a previous publication [26]. From the representative equations reported in the literature for the density [37], isobaric specific heat [38], thermal conductivity [39], and viscosity [40] we find

$$D_T=(0.851\pm0.007)\times10^{-3}\,cm^2\,s^{-1}\,,\qquad \nu=(5.52\pm0.02)\times10^{-3}\,cm^2\,s^{-1} \tag{17}$$

and

$$(A_D^*)_{calc}=(1.22\pm0.02)\times10^{10}\ K^{-2}\,cm^{-2}\,,\qquad (A_\nu^*)_{calc}=(0.189\pm0.002)\times10^{10}\ K^{-2}\,cm^{-2}\,. \tag{18}$$

The experimental correlation-function data are fitted to (15) with (11) substituted for $C(q,t)$ and with D_T and ν fixed at the known values (17) for toluene. The coefficient C_0 in (11) represents the intensity of the equilibrium fluctuations. At a given scattering angle this coefficient is determined from the scattering measurements without a temperature gradient, except that adjustments need to be made for any changes of the incident light intensity and of the local-oscillator strength as discussed previously [25,26]. Hence, in fitting the experimental data to (15), only the background C_B and the amplitudes A_D and A_ν of the nonequilibrium fluctuations are treated as adjustable coefficients. The fits yield standard χ^2 values close to unity confirming that the experimental correlation functions decay indeed with two relaxation times associated with the heat-mode and viscous-mode fluctuations.

The average wave numbers q, the corresponding scattering angles θ, and the spread in wave number δ of the experimental runs are listed in Table I. The first experimental run with $q=2034$ cm^{-1} was performed with the same optical geometry used in the earlier runs with $q=2255$ and 2484 cm^{-1}, so that δ had the value previously determined by Law *et al.* [26]. For the other experimental runs the pinholes were changed as described in Sec. III and the value of δ was adjusted accordingly.

The experimental results obtained for the amplitudes A_D and A_ν are presented in Tables II and III. The errors quoted in these tables represent standard deviations when the results from the fits are averaged over 6–8 individual correlation-function measurements taken with delay times of 2, 4, and 6 μs between the channels of the photon correlator. Only data are included for which no sign of convection was observed. The measurements at $q=2122$ cm^{-1} were not extended to temperature gradients ∇T beyond 100 K/cm because of problems with

TABLE I. Experimental scattering angles, wave numbers, and reduced amplitudes of nonequilibrium fluctuations.

θ (deg)	q (cm^{-1})	δ (cm^{-1})	A_D^* (10^{+10} $K^{-2}cm^{-2}$)	A_ν^* (10^{+10} $K^{-2}cm^{-2}$)
0.45	1528	140	1.233±0.004	0.191±0.002
0.49	1663	140	1.220±0.008	0.198±0.004
0.54	1811	140	1.211±0.006	0.194±0.002
0.61	2034	190	1.180±0.014	0.195±0.003
0.63	2122	140	1.209±0.019[a]	0.185±0.009[a]
0.67	2255	190	1.217±0.011	0.198±0.003
0.74	2484	190	1.209±0.019[a]	0.185±0.009[a]
0.84	2835	140	1.218±0.012	0.195±0.005
		Average:	1.213±0.016	0.194±0.005

[a] From data at $q=2122$ and 2484 cm^{-1} combined.

TABLE II. Experimental nonequilibrium heat-mode amplitude A_D.

∇T (K cm^{-1}) \ q (cm^{-1})	1528±27	1663±35	1811±15	2034±23	2122±82	2255±95	2484±59	2835±24
44.72	4.50±0.11	3.19±0.05	2.33±0.08	1.50±0.04	1.24±0.26	0.78±0.04	0.64±0.05	0.35±0.02
63.25	8.96±0.08	6.65±0.17	4.39±0.10	2.69±0.07	2.32±0.12		1.13±0.06	0.69±0.02
77.46	12.85±0.23	9.05±0.31	7.00±0.07	4.18±0.22	3.13±0.18	3.01±0.18		1.07±0.06
89.44	18.44±0.17	13.07±0.22	8.80±0.08	5.20±0.25	4.69±0.32	3.53±0.06	2.53±0.09	1.49±0.07
100.00	22.87±0.11	16.3±0.5	10.9±0.2	6.85±0.54	6.14±0.11	4.95±0.35	2.89±0.21	1.90±0.08
122.47	32.3±0.7	23.4±0.3	16.3±0.6	11.56±0.43		7.63±0.20		2.85±0.05
141.42	44.8±1.6	31.8±0.5	23.5±0.4	16.23±1.13		10.26±0.45		3.57±0.08
158.11	54.6±0.8	40.7±0.8	29.5±0.5	18.31±0.72				4.72±0.18
173.21	67.0±0.8	47.8±2.1	33.3±0.7	20.68±0.39		13.88±0.26		5.85±0.15
223.61	112.5±2.6	80.4±2.4	54.9±1.0	32.88±0.78		23.60±0.29		9.34±0.12

the laser. An attempt was made to measure the light scattering for each angle at the same ten values of the temperature gradient ∇T. Because of slight variations, of the order 0.1 K, in the temperature of the lower plate, sometimes a small correction was needed to convert the measurements to the desired nominal value of ∇T. In Tables II and III we have also included the experimental amplitudes obtained previously [26] at $q=2255$ and 2484 cm^{-1}, again corrected to the same values of ∇T.

The amplitudes A_D and A_ν represent the strength of the two types of nonequilibrium fluctuations relative to the intensity of the thermal fluctuations in equilibrium. The theory predicts that these amplitudes will be proportional to the square of the temperature gradient and inversely proportional to the fourth power of the wave number in accordance with (12). Our extensive data set enable us to check the dependence on ∇T and q separately.

In Fig. 3 the amplitudes A_d and A_ν obtained at the eight experimental wave numbers are plotted as a function of $(\nabla T)^2$. In Fig. 4 the amplitudes obtained with the ten experimental temperature gradients ∇T are plotted as a function of q^{-4}. The figures confirm that the experimental nonequilibrium amplitudes follow a straight line both when plotted as a function of $(\nabla T)^2$ at constant q and when plotted as a function of q^{-4} at constant ∇T. The solid line in Figs. 3 and 4 represent the theoretically predicted lines with slopes deduced from (12) and (18). These results can be combined by plotting the experimental amplitudes A_D and A_ν as a function of $(\nabla T)^2/q^4$ as was done in previous publications [24,26]. We now cover a range from $(\nabla T)^2/q^4=0.3\times10^{-10}$ to 90×10^{-10} K^2 cm^2. Plots of the amplitudes as a function of $(\nabla T)^2/q^4$ are presented in Figs. 5 and 6. The data do follow a straight line with slopes determined by (18). We emphasize that there are no adjustable parameters in the comparison between experiment and theory.

We note that we have measured nonequilibrium fluctuations with amplitudes A_D and A_ν up to values as large as 112 and 18, respectively. This means we have observed thermal fluctuations in nonequilibrium with a strength two order of magnitude larger than thermal fluctuations in equilibrium. Our smallest wave number $q=1528$ cm^{-1} corresponds to a wave length of about 40 μm. Our experiments provide a dramatic demonstration of the presence of long-range fluctuations in a nonequilibrium system even when the system is not close to a hydrodynamic instability or a critical-point transition.

TABLE III. Experimental nonequilibrium viscous-mode amplitude A_ν.

∇T (K cm^{-1}) \ q (cm^{-1})	1528±27	1663±35	1811±15	2034±23	2122±82	2255±95	2484±59	2835±24
44.72	0.753±0.046	0.521±0.029	0.293±0.013	0.16±0.02	0.20±0.05	0.13±0.08	0.07	0.065±0.020
63.25	1.44±0.05	0.96±0.065	0.638±0.010	0.39±0.01	0.38±0.05		0.19±0.03	0.100±0.025
77.46	2.14±0.11	1.44±0.07	1.05±0.02	0.59±0.05	0.50±0.05	0.44±0.06		0.141±0.029
89.44	2.81±0.06	2.07±0.08	1.36±0.04	0.77±0.05	0.71±0.04	0.53±0.04	0.42±0.04	0.261±0.032
100.00	3.49±0.10	2.57±0.18	1.74±0.11	0.95±0.07	0.92±0.05	0.67±0.06	0.50±0.03	0.303±0.024
122.74	5.12±0.06	3.82±0.30	2.57±0.15	1.75±0.07		1.12±0.08		0.427±0.034
141.42	7.07±0.32	5.32±0.13	3.76±0.05	2.49±0.20		1.51±0.12		0.558±0.025
158.11	8.99±0.36	6.76±0.48	4.68±0.10	2.84±0.14				0.719±0.037
173.21	10.9±0.2	7.74±0.47	5.20±0.24	3.37±0.07		2.24±0.05		0.899±0.034
223.61	18.5±0.9	12.9±1.2	8.98±0.20	5.51±0.27		3.80±0.04		1.534±0.042

To obtain a more detailed measure of the agreement between experiment and theory, we can convert the experimental amplitudes A_D and A_v into reduced amplitudes A_D^* and A_v^* as defined by (12). The experimental values for these reduced amplitudes obtained at the various wave numbers are included in Table I. When the average is taken over all the experimental wave numbers, we obtain

$$A_D^* = (1.213 \pm 0.016) \times 10^{10}\ \mathrm{K}^{-2}\mathrm{cm}^{-2}\ ,$$
$$A_v^* = (0.194 \pm 0.005) \times 10^{10}\ \mathrm{K}^{-2}\mathrm{cm}^{-2}\ . \tag{19}$$

These values agree with the theoretically predicted values (18) within experimental accuracy.

V. TEMPERATURE-DEPENDENT CORRECTIONS

In deriving the theoretical expressions (11) for the nonequilibrium correlation functions we have neglected any spatial variations of the thermophysical properties of the liquid resulting from the imposed temperature gradient [15,41]. The question arises whether the approximation remains valid when the temperature gradient becomes as large as about 200 K/cm used in our experiments.

For the theory to be valid we demand that the spatial variations of the properties are negligibly small over distances of the order of the wavelength of the fluctuations. In our experiments we have probed fluctuations with wavelengths up to 40 μm. Over such distances the temperature varies by less than 1 °C, so that the properties can indeed be identified with their values at the local temperature T. Hence Eq. (11) should be interpreted as

$$C(q,t) = C_B(1 + C_0(T)\{[1 + A_D(T)]\exp[-D_T(T)q^2 t] - A_v(T)\exp[-\nu(T)q^2 t]\})\ . \tag{20}$$

The amplitudes $A_D(T)$ and $A_v(T)$ depend on the local temperature through the coefficients A_D^* and A_v^* given in (13), while the amplitude $C_0(T)$ of the equilibrium fluctuations is proportional to [29]

$$C_0 \propto \left[\frac{\partial \rho}{\partial s}\right]_p^2 \frac{k_B c_p}{\rho} = \left[\frac{T\rho\alpha_T}{c_p}\right]^2 \frac{k_B c_p}{\rho}\ , \tag{21}$$

where $\alpha_T = \rho^{-1}(\partial\rho/\partial T)_p$ is the thermal expansion coefficient.

In the actual experiments we measure the fluctuations

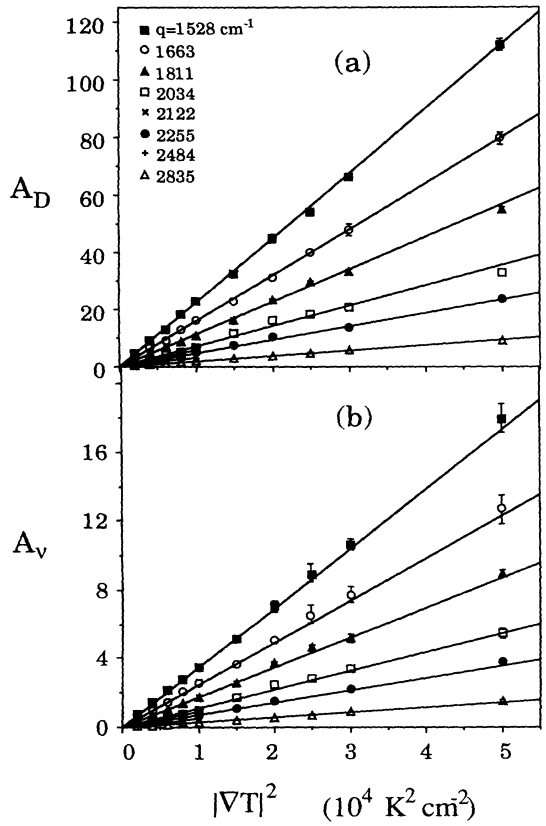

FIG. 3. Amplitudes A_D and A_v of the nonequilibrium fluctuations as a function of $(\nabla T)^2$ at various wave numbers. The lines represent the values predicted theoretically.

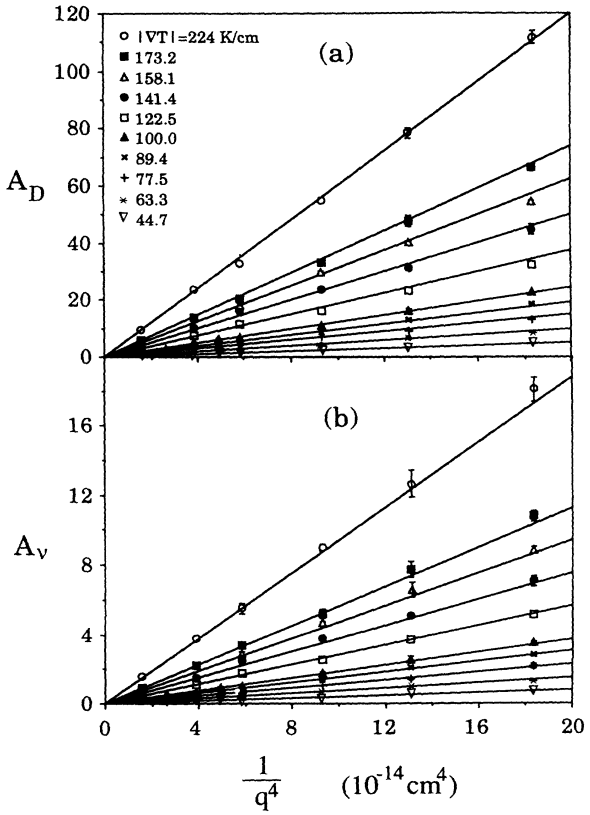

FIG. 4. Amplitudes A_D and A_v of the nonequilibrium fluctuations as a function of q^{-4} at various values of the temperature gradient. The lines represent the values predicted theoretically.

averaged over a finite scattering volume. For the small scattering angles used, the height of this scattering volume spans the entire height of 2 mm of the liquid layer. While the average temperature was maintained at 40 °C, a gradient of 200 K/cm implies that the actual temperature varies from 20 to 60 °C. The variation of the coefficients $C_0(T)$, $A_D^*(T)$, $A_\nu^*(T)$, $D_T(T)$, and $\nu(T)$ with temperature, as calculated from the known temperature dependence of the properties of toluene [37–40], is shown in Fig. 7. In the analysis of the experimental results, presented in Sec. IV, we have identified these coefficients with their values at the average temperature $\bar{T}=313.15$ K (i.e., 40 °C). However, for $\nabla T=200$ K/cm the variations of these coefficients become substantial, e.g., A_D^* varies by ±30% and A_ν^* by ±45%. To account for these variations we substitute (20) into (15) and average over the experimental temperature range from $T=T_1$ at the lower plate, to $T=T_2$ at the upper plate:

$$\bar{C}(q,t)=C_B\{1+C_0(\bar{T})[R_{\rm eq}(q,T,t)+A_D(\bar{T})R_D(q,T,t)]e^{-D_T(\bar{T})q^2t} - C_0(\bar{T})A_\nu(\bar{T})R_\nu(q,T,t)e^{-\nu(\bar{T})q^2t}\} . \tag{22}$$

where

$$R_{\rm eq}(q,T,t)=\frac{e^{D_T(\bar{T})q^2t}}{Z(T_2-T_1)} \times\int_{q-3\delta}^{q+3\delta}dq'e^{-(q'-q)^2/2\delta^2} \times\int_{T_1}^{T_2}dT\,\tilde{C}_0(T)e^{-D_T(T)q^2t}, \tag{23}$$

$$R_D(q,T,t)=q^4\frac{e^{D_T(\bar{T})q^2t}}{Z(T_2-T_1)} \times\int_{q-3\delta}^{q+3\delta}dq'(q')^{-4}e^{-(q'-q)^2/2\delta^2} \times\int_{T_1}^{T_2}dT\,\tilde{C}_0(T)\tilde{A}_D^*(T)e^{-D_T(T)q^2t}, \tag{24}$$

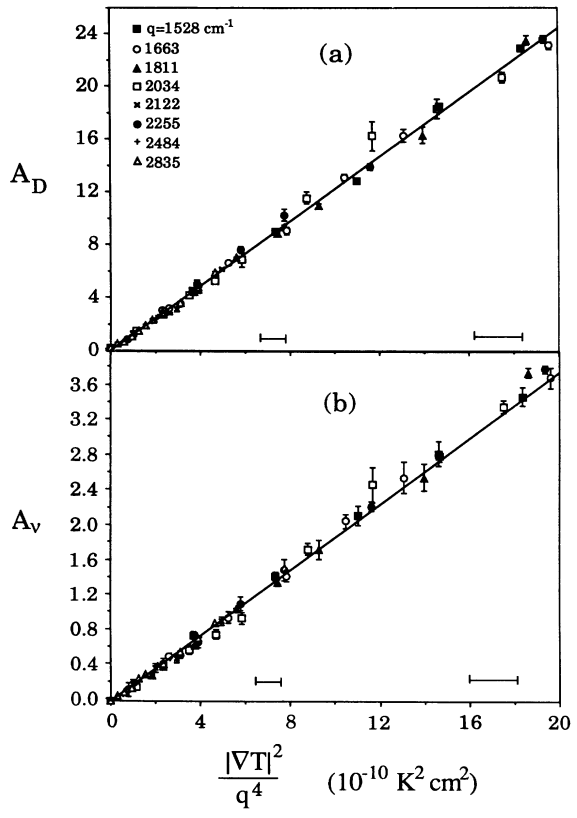

FIG. 5. Amplitudes A_D and A_ν of the nonequilibrium fluctuations as a function of $(\nabla T)^2q^4$. The lines represent the values predicted theoretically.

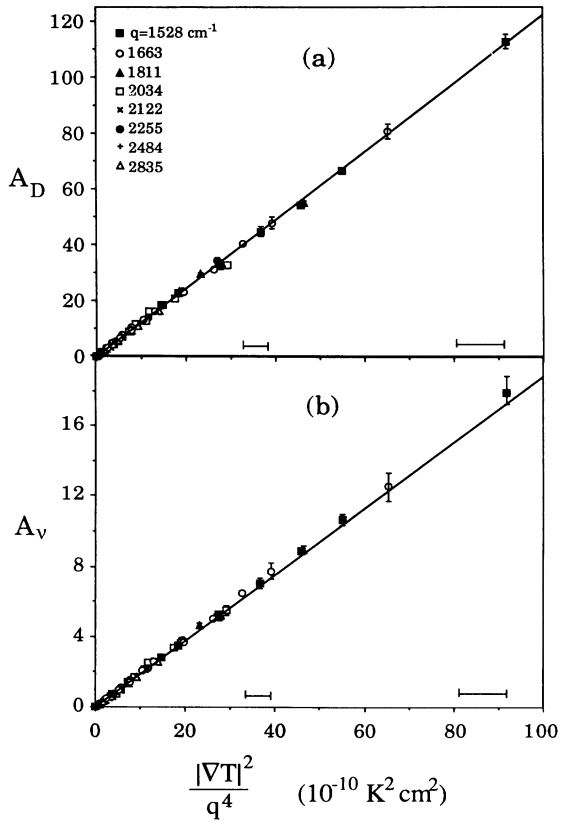

FIG. 6. Amplitudes A_D and A_ν of the nonequilibrium fluctuations as a function of $(\nabla T)^2/q^4$. The lines represent the values predicted theoretically.

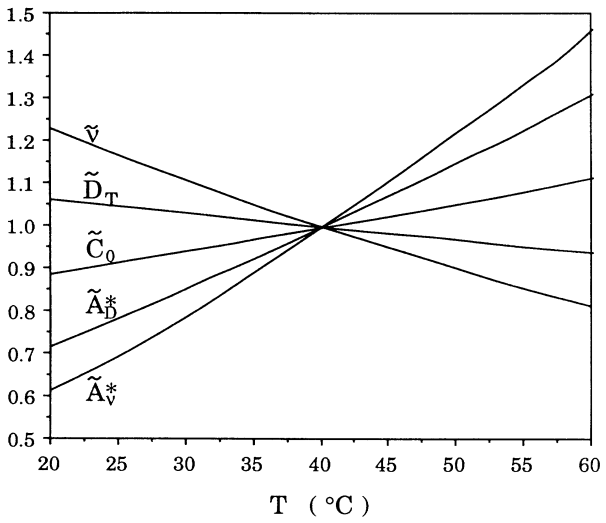

FIG. 7. The coefficients $\tilde{X}(T)=X(T)/X(\bar{T})$ of toluene as a function of temperature ($X=C_0$, A_D^*, A_ν^*, D_T and ν).

$$R_\nu(q,T,t)=q^4\frac{e^{\nu(\bar{T})q^2t}}{Z(T_2-T_1)}\times\int_{q-3\delta}^{q+3\delta}dq'(q')^{-4}e^{-(q'-q)^2/2\delta^2}\times\int_{T_1}^{T_2}dT\,\tilde{C}_0(T)\tilde{A}_\nu^*(T)e^{-\nu(T)q^2t}, \tag{25}$$

with

$$\tilde{C}_0(T)=\frac{C_0(T)}{C_0(\bar{T})},\quad \tilde{A}_D^*(T)=\frac{A_D^*(T)}{A_D^*(\bar{T})},\quad \tilde{A}_\nu^*(T)=\frac{A_\nu^*(T)}{A_\nu^*(\bar{T})}. \tag{26}$$

Here $R_{eq}(q,T,t)$, $R_D(q,T,t)$, and $R_\nu(q,T,t)$ represent the correction factors to the equilibrium correlation function, to the nonequilibrium heat-mode correlation function, and to the nonequilibrium viscous-mode correlation function, respectively. The integrals (23)–(25) can be readily evaluated from the known temperature dependence of the properties of toluene as shown in Fig. 7. In practice we evaluated these integrals numerically as a double sum over 37 equally spaced scattering angles corresponding to the range of wave numbers from $q-3\delta$ to $q+3\delta$ and over 67 equidistant positions along the vertical axis in the liquid layer. It is noted that the temperature profile in the liquid layer is not linear, since the thermal-conductivity coefficient also depends on temperature. In the absence of any fluid motion the heat-conduction equation becomes

$$\rho c_p\frac{\partial T}{\partial t}\nabla(\lambda\nabla T). \tag{27}$$

Since in the steady state $\partial T/\partial t=0$ everywhere, the temperature profile is determined from the condition

$$(\nabla\lambda)(\nabla T)+\lambda\nabla^2T=0. \tag{28}$$

As an example we show in Fig. 8 the correction factors $R_{eq}(q,T,t)$, $R_D(q,T,t)$, and $R_\nu(q,T,t)$ as a function of the thermal and viscous-mode decay times for the case where $q=2835\ \text{cm}^{-1}$, $\delta=140\ \text{cm}^{-1}$ and $\nabla T=158\ \text{K/cm}$. In addition we show the correction factors $R_{eq}(q,t)$, $R_D(q,t)$, and $R_\nu(q,t)$ if the temperature variations of the properties are neglected, as was done in Sec. IV. From Fig. 8 we note that the effects of these corrections on the equilibrium correlation function are negligibly small. However, both the spread of wave numbers and the temperature dependence of the properties do affect the nonequilibrium contributions to the correlation functions. The nonequilibrium viscous-mode contributions are most strongly affected due to the strong temperature dependence of the kinematic viscosity ν.

The analysis of the experimental data now proceeds in a manner completely analogous to that described in Sec. IV. First the coefficient $C_0(\bar{T})$ and the wave number q in (22) are determined from the experimental correlation

TABLE IV. Nonequilibrium thermal-mode amplitude A_D after correcting for temperature effects.

∇T (K cm^{-1}) \ q (cm^{-1})	1528±27	1663±35	1811±15	2255±95	2835±24
44.72	4.49±0.11	3.19±0.05	2.31±0.07	0.78±0.04	0.35±0.02
63.25	8.96±0.06	6.63±0.18	4.38±0.10		0.68±0.02
77.46	12.81±0.23	9.02±0.32	6.97±0.07	3.00±0.18	1.07±0.06
89.44	18.32±0.18	12.90±0.20	8.77±0.09	3.50±0.06	1.48±0.07
100.00	22.73±0.09	16.10±0.70	10.90±0.09	4.96±0.33	1.88±0.08
122.47	32.0±0.6	23.30±0.50	16.3±0.5	7.61±0.18	2.82±0.06
141.42	44.4±1.5	31.6±1.0	23.1±0.2	10.17±0.46	3.53±0.08
158.11	54.2±0.8	40.6±0.4	29.5±0.5		4.67±0.18
173.21	66.9±0.6	47.7±1.9	33.1±0.7	13.78±0.26	5.79±0.26
223.61	112.6±1.7	79.8±0.9	54.6±1.1	23.25±0.33	9.20±0.14

TABLE V. Nonequilibrium viscous-mode amplitude A_v after correcting for temperature effects.

∇T (K cm^{-1}) \ q (cm^{-1})	1528±27	1663±35	1811±15	2255±95	2835±24
44.72	0.750±0.056	0.533±0.044	0.288±0.015	0.13±0.07	0.062±0.022
63.25	1.45±0.07	0.959±0.068	0.637±0.009		0.099±0.022
77.46	2.14±0.11	1.44±0.08	1.04±0.02	0.43±0.06	0.139±0.029
89.44	2.77±0.05	2.05±0.08	1.34±0.05	0.52±0.04	0.258±0.029
100.00	3.43±0.09	2.51±0.26	1.73±0.09	0.67±0.06	0.295±0.026
122.47	5.01±0.17	3.78±0.24	2.56±0.14	1.10±0.07	0.420±0.024
141.42	6.77±0.27	5.25±0.48	3.74±0.07	1.47±0.12	0.542±0.027
158.11	8.87±0.31	6.69±0.38	4.66±0.05		0.698±0.041
173.21	10.8±0.2	7.73±0.38	5.10±0.27	2.21±0.05	0.866±0.036
223.61	18.4±0.6	12.9±0.8	8.84±0.33	3.70±0.05	1.45±0.059

function data obtained with $\nabla T=0$. Then the experimental nonequilibrium correlation-function data are fitted to Eq. (22) yielding the background C_B and the nonequilibrium amplitudes $A_D(\bar{T})$ and $A_v(\bar{T})$.

As an example we present in Tables IV and V the nonequilibrium amplitudes $A_D(\bar{T})$ and $A_v(\bar{T})$ thus deduced from the light-scattering measurements at $q=1528$, 1663, 1811, 2255, and 2835 cm^{-1}; these data are to be compared with the corresponding entries in Tables II and III. The temperature correction increases of course with increasing values of the temperature gradient ∇T; it also increases with increasing values of the wave number q. For the nonequilibrium heat-mode amplitude A_D the correction remains small up to a maximum value of about 1% at the largest temperature gradient. For the nonequilibrium viscous-mode amplitude A_v the corrections become larger up to a value of 6%.

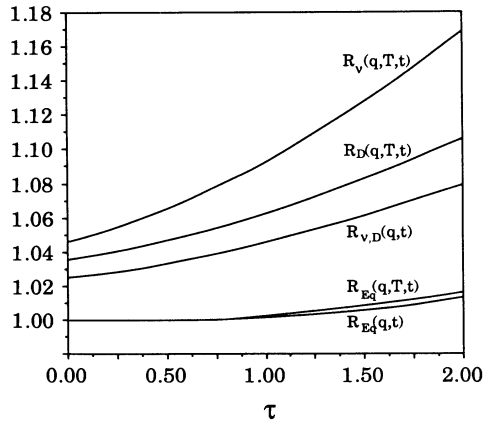

FIG. 8. The correction factors R_{eq}, R_D, and R_v for the equilibrium and nonequilibrium contributions to the correlation function for $q=2835$ cm^{-1}, $\delta=140$ cm^{-1}, and $\nabla T=158$ K/cm. The correction factors are plotted as a function of the time relative to the corresponding decay time $\tau=t/t_D$ and t/t_v, where $t_D=1/D_T q^2$ and $t_v=1/\nu q^2$ ($t_D\approx 147$ μs and $t_v\approx 23$ μs). $R_{eq}(q,t)$, $R_D(q,t)$, and $R_v(q,t)$ are the correction factors if only the spread in wave numbers is taken into account. $R_{eq}(q,T,t)$, $R_D(q,T,t)$, and $R_v(q,T,t)$ are the correction factors if also the temperature variation of the properties of toluene is taken into account.

The values obtained for the reduced amplitudes $A_D^*(\bar{T})$ and $A_\mu^*(\bar{T})$ are presented in Table VI, to be compared with the values previously presented in Table I. The effect of the temperature corrections is to yield a slightly smaller spread in the obtained amplitude ratios, but otherwise they are insignificant. From the information in Table VI we conclude

$$(A_D^*)_{calc}=(1.213\pm 0.014)\times 10^{10}\ \mathrm{K}^{-2}\mathrm{cm}^{-2}\ ,$$
$$(A_v^*)_{calc}=(0.192\pm 0.004)\times 10^{10}\ \mathrm{K}^{-2}\mathrm{cm}^{-2}\ , \tag{29}$$

to be compared with the predicted values (18). The temperature dependence of the properties of the liquid yields a small correction to the amplitude of the nonequilibrium viscous-mode contributions which leads to even better agreement with the theory.

VI. CONCLUSIONS

We have obtained Rayleigh-scattering data for liquid toluene subjected to a stationary temperature gradient ∇T. The measurements cover wave numbers from 1528 to 2835 cm^{-1} and temperature gradients up to $\nabla T=224$ K/cm. The experiments show the presence of long-range heat-mode and viscous-mode nonequilibrium fluctuations. In a previous publication [26] we verified the

TABLE VI. Reduced nonequilibrium amplitudes $A_D^*(\bar{T})$ and $A_v^*(\bar{T})$ after correcting for temperature effects.

q (cm^{-1})	$A_D^*(\bar{T})$ (10^{+10}K^{-2}cm^{-2})	$A_v^*(\bar{T})$ (10^{+10} K^{-2}cm^{-2})
1528	1.277±0.004	0.191±0.002
1663	1.227±0.007	0.195±0.004
1811	1.207±0.005	0.195±0.002
2255	1.207±0.012	0.193±0.003
2835	1.196±0.013	0.185±0.006
Average:	1.213±0.014	0.192±0.004

dependence of the strength of these nonequilibrium fluctuations on $(\nabla T)^2/q^4$. From the set of data presented here, covering a larger range of wave numbers we have checked both the dependence on ∇T and the dependence on q^{-4}. The observed amplitudes of the nonequilibrium fluctuations are in excellent quantitative agreement with the values predicted from fluctuating hydrodynamics.

ACKNOWLEDGMENTS

The authors acknowledge valuable discussions with E. G. D. Cohen, T. R. Kirkpatrick, and R. Schmitz. They are also indebted to M. Lamvik for experimental assistance. The research was supported by National Science Foundation Grant No. DMR-8814439.

[1] L. Landau and G. Placzek, Phys. Z. Sov. **5**, 1972 (1934).
[2] R. F. Fox, J. Phys. Chem. **86**, 2812 (1982).
[3] A. -M. S. Tremblay, in *Recent Developments in Nonequilibrium Thermodynamics,* edited by J. Casas-Vazquez, D. Jou, and G. Lebon, Lecture Notes in Physics Vol. 199 (Springer Verlag, Berlin, 1984), p. 267.
[4] R. Schmitz, Phys. Rep. **171**, 1 (1988).
[5] D. Beysens, Y. Garrabos, and G. Zalczer, Phys. Rev. Lett. **45**, 403 (1980).
[6] H. Kiefte, M. J. Clouter, and R. Penney, Phys. Rev. B **30**, 4017 (1984).
[7] G. Satten and D. Ronis, Phys. Rev. A **26**, 940 (1982).
[8] R. Schmitz and E. G. D. Cohen, J. Stat. Phys. **46**, 319 (1987).
[9] R. Schmitz and E. G. D. Cohen, Phys. Rev. A **35**, 2602 (1987).
[10] R. Schmitz, J. Stat. Phys. **57**, 549 (1989).
[11] T. R. Kirkpatrick, E. G. D. Cohen, and J. R. Dorfman, Phys. Rev. A **26**, 995 (1982).
[12] L. P. Kadanoff and J. Swift, Phys. Rev. **166**, 89 (1968).
[13] K. Kawasaki, in *Phase Transitions and Critical Phenomena,* edited by C. Domb and M. S. Green (Academic, New York, 1976), Vol. 5A, p. 165.
[14] M. H. Ernst, E. H. Hauge, and J. M. J. van Leeuwen, Phys. Lett. **34A**, 419 (1971).
[15] D. Ronis and I. Procaccia, Phys. Rev. A **26**, 1812 (1982).
[16] R. Schmitz and E. G. D. Cohen, J. State Phys. **39**, 285 (1985); **40**, 431 (1985).
[17] B. M. Law and J. V. Sengers, J. Stat. Phys. **57**, 531 (1989).
[18] I. L'Heureux and I. Oppenheim, Physica A **148**, 503 (1988).
[19] H. Spohn, J. Phys. A **16**, 4275 (1983).
[20] G. Nicolis and M. Malek Mansour, Phys. Rev. A **29**, 2845 (1984).
[21] M. Q. Zhang, J. S. Wang, J. L. Lebowitz, and J. L. Vallés, J. Stat. Phys. **52**, 1461 (1988).
[22] P. G. Garrido, J. L. Lebowitz, C. Maes, and H. Spohn, Phys. Rev. A **42**, 1954 (1990).
[23] G. Grinstein, J. Appl. Phys. **8**, 5441 (1991).
[24] B. M. Law, R. W. Gammon, and J. V. Sengers, Phys. Rev. Lett. **60**, 1554 (1988).
[25] B. M. Law, R. W. Gammon, and J. V. Sengers, in *OSA Proceedings on Photon Correlation Techniques and Applications,* edited by J. B. Abbiss and A. E. Smart (Optical Society of America, Washington, DC, 1988), Vol. 1, p. 147.
[26] B. M. Law, P. N. Segrè, R. W. Gammon, and J. V. Sengers, Phys. Rev. **41**, 816 (1990).
[27] R. D. Mountain, Rev. Mod. Phys. **38**, 205 (1966).
[28] D. McIntyre and J. V. Sengers, in *Physics in Simple Liquids,* edited by H. N. V. Temperley, J. S. Rowlinson, and G. S. Rushbrooke (North-Holland, Amsterdam, 1968), p. 447.
[29] J. V. Sengers and B. M. Law, in *Lectures on Thermodynamics and Statistical Mechanics,* edited by M. Lòpez de Haro and C. Varea (World Scientific, Singapore, 1990), p. 201.
[30] L. D. Landau and E. M. Lifschitz, *Fluid Mechanics* (Addison-Wesley, Reading, MA, 1959), Chap. XVIII.
[31] Y. M. Kim (private communication).
[32] M. Hendrix, A. Leipertz, M. Fiebig, and G. Simonsohn, Int. J. Heat Mass Transfer **30**, 333 (1987).
[33] J. N. Shaumeyer, R. W. Gammon, and J. V. Sengers, in *Experimental Thermodynamics III: The Measurement of Transport Properties of Fluids,* edited by W. A. Wakeham, A. Nagashima, and J. V. Sengers (Blackwell Scientific, Oxford, 1991)
[34] H. C. Burstyn, Rev. Sci. Instrum. **51**, 1431 (1980).
[35] M. Corti and V. Degiorgio, J. Phys. C **8**, 953 (1975).
[36] P. N. Pusey, J. M. Vaughan, and D. V. Willets, J. Opt. Soc. Am. **73**, 1012 (1983).
[37] H. Kashiwagi, T. Hashimoto, Y. Tanaka, H. Kubota, and T. Makita, Int. J. Thermophys. **3**, 201 (1982).
[38] D. W. Scott, G. B. Guthrie, J. F. Messerly, S. S. Todd, W. T. Berg, I. A. Hossenlopp, and J. P. McCullough, J. Phys. Chem. **66**, 911 (1962).
[39] C. A. Nieto de Castro, S. F. Y. Li, A. Nagashima, R. D. Trengrove, and W. A. Wakeham, J. Phys. Chem. Ref. Data **15**, 1073 (1986).
[40] F. A. Gonçalves, K. Hamano, J. V. Sengers, and J. Kestin, Int. J. Thermophys. **8**, 641 (1987).
[41] A. -M. S. Tremblay, M. Arai, and E. D. Siggia, Phys. Rev. A **23**, 1451 (1981).